Environmental Science and Pollution Research (2018) 25:33783–33793
https://doi.org/10.1007/s11356-018-3309-z

RESEARCH ARTICLE

Characteristics and source apportionment of winter black carbon aerosols in two Chinese megacities of Xi'an and Hong Kong

Qian Zhang[1,2] · Zhenxing Shen[2,3] · Zhi Ning[4] · Qiyuan Wang[3] · Junji Cao[3] · Yali Lei[2] · Jian Sun[2] · Yaling Zeng[2] · Dane Westerdahl[4] · Xin Wang[2] · Linqing Wang[2] · Hongmei Xu[2]

Received: 21 February 2018 / Accepted: 20 September 2018 / Published online: 2 October 2018

Abstract

Black carbon (BC) aerosols were observed over Xi'an (XA) and Hong Kong (HK) to better compare its properties and sources in two geographically separate regions in China. High-BC (7.9 ± 3.3 μg·m^{-3}) and -$PM_{2.5}$ (182 ± 80.5 μg·m^{-3}) concentrations were observed in XA, and these were much higher than those in HK (BC, 3.2 ± 0.9 μg·m^{-3}; $PM_{2.5}$, 34.5 ± 9.3 μg·m^{-3}). The contribution of BC to $PM_{2.5}$ in HK reached 10.7%, which was ~ 1.5 times than that in XA (7.6%). The results emphasized that BC played an important role in HK $PM_{2.5}$. The diurnal distribution of HK BC was highly correlated with vehicle emissions during the daytime; it peaked during heavy traffic times. Whereas XA BC exhibited flat distribution owing to stable BC sources. It is not markedly driven by traffic patterns. Additionally, the potential source contribution function (PSCF) analysis showed that XA BC mainly originated from local emissions while nearly half of the HK BC originated from distant sources, such as industrial emissions from northeastern regions and ship emissions from marine regions. These anthropogenic BC sources were found to be regional in nature based on multilinear engine (ME-2) analysis. Specifically, the XA BC sources were dominated by three factors: 22.5% from coal burning, 19.6% from biomass burning, and 32.9% from vehicle emissions. In HK, the majority of BC contributions originated from vehicle and ship emissions (78.9%), while only 14.5% and 1.5% originated from coal and biomass burning from residential combustion, as well as industrial and power plants in inland China.

Keywords Black carbon · Urban atmosphere · Potential source contribution function · Multilinear engine · Source identification

Introduction

Black carbon (BC) emissions have caused environmental concerns, contributed to climate change on local, regional, and worldwide scales, and have become a major focus for research (Bond et al. 2013; Ding et al. 2016; Cooke and Wilson 1996; Ramanathan and Carmichael 2008). BC can be used as a primary tracer for the anthropogenic pollution sources of fossil fuel combustion and biomass burning, because it is abundant in the combustion of carbon-based fuels when oxygen is insufficient and can also be produced when adequate oxygen is present in combustion with poorly mixed reactants (Reddy et al. 2002; Cooke and Wilson 1996). WHO (2012) reported that severe BC pollution has also attracted considerable scientific concern because of its effects on public health. In the study of Shindell et al. (2012), the global health benefits of USD 5142 billion from

Responsible editor: Constantini Samara

Electronic supplementary material The online version of this article (https://doi.org/10.1007/s11356-018-3309-z) contains supplementary material, which is available to authorized users.

✉ Zhenxing Shen
zxshen@mail.xjtu.edu.cn

[1] School of Environmental & Municipal Engineering, Xi'an University of Architecture and Technology, Xi'an 710055, China

[2] Department of Environmental Science and Engineering, Xi'an Jiaotong University, Xi'an 710049, China

[3] Key Lab of Aerosol Chemistry & Physics, Institute of Earth Environment, Chinese Academy of Sciences, Xi'an, China

[4] School of Energy and Environment, City University of Hong Kong, Hong Kong, China

the reduction of BC were estimated which were far larger than those from CH_4 in the year 2030 due to the implementation of several BC measures. Scientists have conducted many experiments to identify the specific role of BC in environmental problems and have determined that it is a dominant contributor to visibility degradation through light absorption (Lee and Sequeira 2002; Lin et al. 2014; Huang et al. 2012). In general, BC particles absorb visible and infrared wavelengths in the atmosphere and among carbonaceous aerosols are second only to CO_2 in their production of a positive force of + 0.2 to + 1.1 $W{\cdot}m^{-2}$ (Lloyd and Cackette 2001; Ramanathan and Carmichael 2008). BC radiative forcing values vary among source combustions, such as those of fossil fuel (+ 0.29 $W{\cdot}m^{-2}$), biofuel (+ 0.22 $W{\cdot}m^{-2}$), and open burning (+ 0.20 $W{\cdot}m^{-2}$) (Li et al. 2016). Moreover, BC plays a significant role in severe air pollution; in their studies, both Kirchstetter et al. (2008) and Allen et al. (1999) observed similar and significant linear relationships ($R > 0.98$, $P < 0.001$) between BC and coefficient of haze.

Wang et al. (2014) reconstructed emission inventories using a bottom-up approach based on 64 sources, and identified an increasing trend in total global emissions of BC since 1960 that reached 9000 $Gg{\cdot}year^{-1}$ in 2007. Numerous studies have confirmed that the distributions and characteristics of BC differ among regions according to the specific sources of BC. For example, a study determined that approximately 64% of global BC emissions originated from various sources in the open environment, such as burning forests, grasslands, and agricultural residues. Approximately, 60–80% of BC emissions were produced by the residential combustion of coal and biofuels in Asia and Africa, and 70% were generated by fresh and aged diesel combustion in traffic-dominated areas in Europe (Bond et al. 2013; Wang et al. 2014). BC emissions in Asia caused direct radiative forcing three times higher than that in Europe. In China, annual BC emissions have increased constantly since 1960 because of increasing emissions from residential-, industrial-, and motor vehicle-related combustion (Wang et al. 2012a). Scientists modeled the trend of total BC emissions in China from 1949 to 2050, which estimated that the BC emissions would increase to a peak value of 2273 $Gg{\cdot}year^{-1}$ in 2041 due to the increase of anthropogenic BC emissions by factors of 1.6–3.6, including motor vehicles, off-road diesel machineries, coal combustions, and industrial productions (Wang et al. 2012b).

Although previous studies have examined temporal and spatial variations in BC concentrations in several individual Chinese urban areas, few studies have observed or comparatively analyzed data from various areas of China with regard to the emission sources (Ding et al. 2016; Pérez et al. 2010; Wang et al. 2015; Zhang et al. 2015). To characterize the distribution and sources of BC in urban atmospheres in China, this study investigated the temporal and spatial distribution of BC in two geographically distinct parts of China, Xi'an (XA) and Hong Kong (HK), in 2016. To understand the BC sources and transport paths, we modeled the relationship between the concentration of BC and meteorological parameters and determined and compared the transport pathways and possible sources of BC for XA and HK using the potential source contribution function. Finally, an advanced source analysis model of multilinear engine 2 (ME-2) was used to quantify the source contributors of BC in XA and HK.

Methodology

Sampling site

We conducted field observations in two representative sites for two geographically separate regions in China XA and HK to better compare the BC properties and sources (Fig. 1). One was a typical urban near-source roadside site in HK representing the relatively fresh emissions from combustion sources and the other was a typical urban ambient site near downtown of XA, China, which is heavily affected by abundant combustion emissions from local and regional sources. Both sites have been included in our previous investigations:

XA site: The site is located in the southeast area of downtown XA (34° 16′ N, 108° 54′ E) that is surrounded by complex sources. Residential areas and the campus of Xi'an Jiaotong University are nearby. Two roads with heavy traffic (the South Second Ring and Xingqing Road) include large number of diesel-powered trucks and busses (Shen et al. 2012; Zhang et al. 2015).

HK site: The site is situated about 5 m away from the curb of Lai Chi Kok (LCK) Road in HK (22° 19′ N, 114° 9′ E), one of the busiest traffic arteries in the city, with average vehicle counts of 5000–6000 per hour and diesel vehicles accounting for nearly 40% of the traffic volume (Cheng et al. 2010; Ning et al. 2013). Moreover, residential buildings of 8–10 stories bound both sides of this site. This topography is typical of the city and results in street canyon effects and suppressed dispersion of on-road emissions.

BC measurement and source identification

Real-time BC measurement was conducted during the sampling periods. The BC concentration was determined using a seven-wavelength Aethalometer-31 (Model-AE31, Magee Scientific Inc., USA). The AE31 flow rate was calibrated prior to deployment in the field and the sampling air flow rate was 5.0 $L{\cdot}min^{-1}$. The AE31 was programmed to automatically measure the light attenuation (ATN) at seven wavelengths (370, 470, 520, 590, 660, 880, and 950 nm) in micrograms per cubic meter at 5-min intervals over the sampling period from a location near the $PM_{2.5}$ samplers. The ATN data from

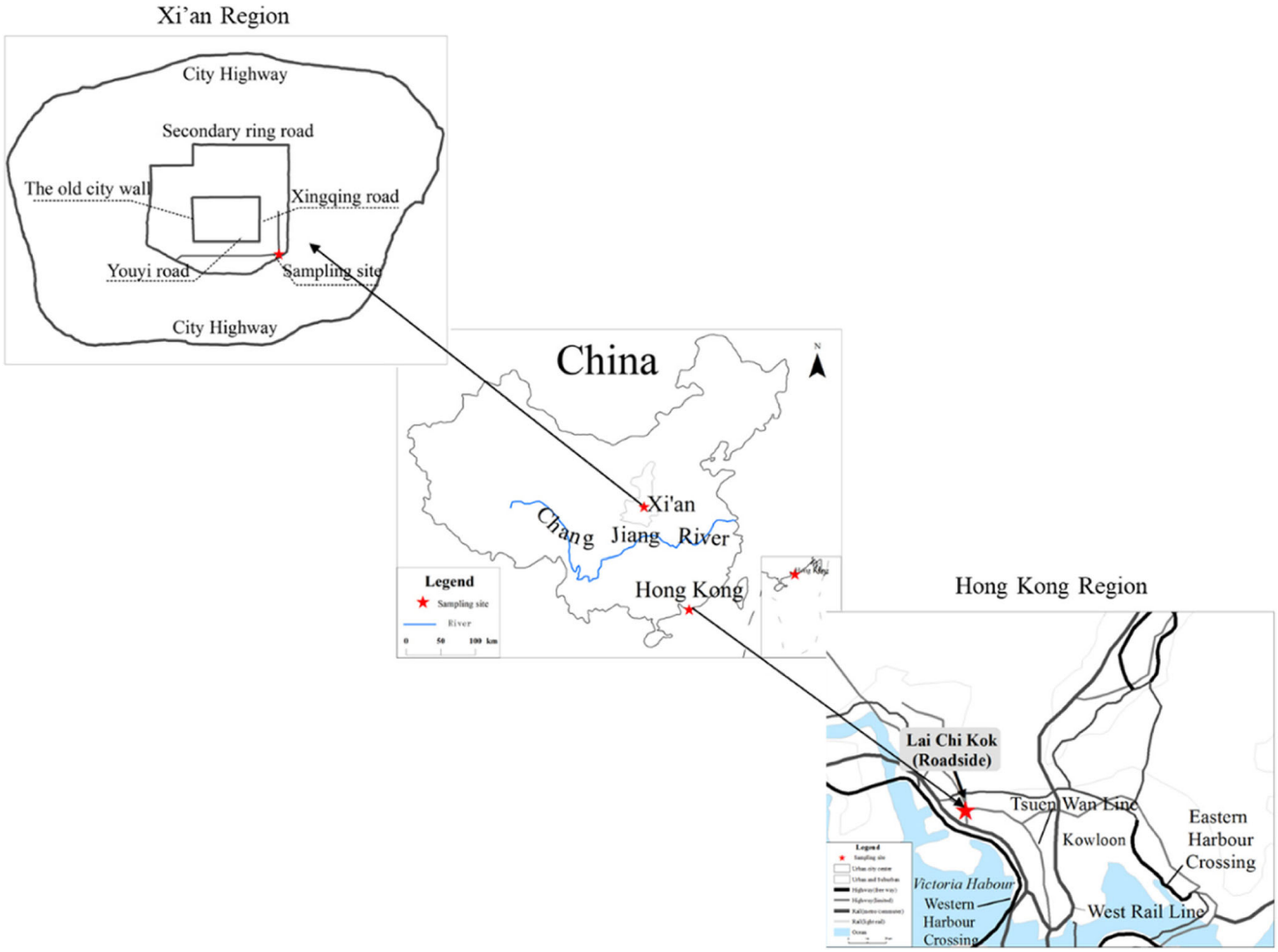

Fig. 1 The location of the sampling site for parallel observations between Xi'an and Hong Kong

the AE31 are converted to BC mass by assuming a fixed BC-specific attenuation coefficient (σ) at 880 nm of 16.6 $m^2 \cdot g^{-1}$ (Virkkula et al. 2007). The accuracy of BC data from the Aethalometer is impacted by two factors: non-linear response as loading levels on the filter media increase (loading factor) and light scattering by the fiber filter substrates (Collaud et al. 2010). These factors were considered and corrected as described in a study of Shen et al. (2017).

The light absorption coefficient (b_{abs}), which is the most important parameter for BC determination, can be obtained from AE31 (Zhang et al. 2017). Sandradewi et al. (2008) built the Aethalometer model using b_{abs} and absorption Angstrom exponent (AAE, which indicates the spectral dependence) data to quantify the contributions of two typical BC sources (includes fossil fuel burning (BC_FF) and biomass burning (BC_BB)) to total BC concentrations. Healy et al. (2017) segregated b_{abs_FF} and b_{abs_BB} by projecting the absorption at higher wavelengths (880 nm) to lower wavelengths of the spectrum measured by the AE31. The b_{abs} values at 880 nm and 370 nm were assumed to be the sum of b_{abs}_FF and b_{abs}_BB, respectively. The simple extrapolation method using an AAE has been described in detail by Healy et al. (2017). We get the following equations:

$$\frac{b_{abs}(370\text{nm})_{FF}}{b_{abs}(880\text{nm})_{FF}} = \left(\frac{370}{880}\right)^{-(AAE\_FF)} \quad (1)$$

$$\frac{b_{abs}(370\text{nm})_{BB}}{b_{abs}(880\text{nm})_{BB}} = \left(\frac{370}{880}\right)^{-(AAE\_BB)} \quad (2)$$

$$b_{abs}(370\text{nm}) = b_{abs}(370\text{nm})_{FF} + b_{abs}(370\text{nm})_{BB} \quad (3)$$

$$b_{abs}(880\text{nm}) = b_{abs}(880\text{nm})_{FF} + b_{abs}(880\text{nm})_{BB} \quad (4)$$

$$BC_{FF} = \frac{b_{abs}(880\text{nm})_{BB}}{\sigma_{880\text{nm}}} \quad (5)$$

$$BC = BC\_FF + BC\_BB \quad (6)$$

where $b_{abs}(\lambda)$ is the absorption coefficient, λ is the wavelength, $b_{abs}(\lambda)_{FF}$ a fossil fuel fraction, and $b_{abs}(\lambda)_{BB}$ a biomass burning fraction of absorption coefficient. In this equation, b_{abs} is expressed in the unit of Mm^{-1} (or 10^{-6} m^{-1}), while the AAE_FF = 0.9 for fossil fuel and AAE_BB = 2.09 for biomass burning (Zotter et al. 2017). σ_{880nm} here refers to the

attenuation coefficient of BC (16.6 $m^2 \cdot g^{-1}$) at the wavelength of 880 nm.

$PM_{2.5}$ collection and chemical analysis

For parallel sampling, ambient 24-h (10:00 a.m.–10:00 a.m., + 1 day) $PM_{2.5}$ samples were simultaneously collected over XA and HK on Whatman 47 quartz filters (Whatman Inc., Maidstone, UK) using a MiniVol ambient air particulate sampler (BGI Inc., USA) at a flow rate of 5 $L \cdot min^{-1}$ from 15 Dec. 2016 to 15 Jan. 2017. The filter samples were weighed three times on a high-precision (± 1 μg) microbalance (ME-5, Sartorius Inc., Germany) to determine PM mass. After weighing, all samples were stored in a freezer at − 20 °C to prevent the evaporation of volatile compounds (Shen et al. 2016).

A 0.5-cm^2 punch of each sample was analyzed for Thermo-EC and OC of $PM_{2.5}$ in this study following the Interagency Monitoring of Protected Visual Environments (IMPROVE) thermal/optical reflectance (TOR) protocol using a DRI Model 2001 Thermal and Optical Carbon Analyzer (Atmoslytic Inc., California, USA). Four OC fractions (OC1, OC2, OC3, and OC4 at 140 °C, 280 °C, 480 °C, and 580 °C, respectively, in a helium atmosphere) and three EC fractions (EC1, EC2, and EC3 at 580 °C, 740 °C, and 840 °C, respectively, in a 2% oxygen/98% helium atmosphere) were also determined. During volatilization of organic carbon, part of the organic carbon was converted pyrolytically to EC (this fraction of OC was named as OP) (Chow et al. 2004). Hence, OC is the sum of OC1, OC2, OC3, OC4, and OP, and EC is the sum of EC1, EC2, and EC3 and then minus OP. Additional quality assurance and quality control procedures have been described in detail by Cao et al. (2003). In general, BC and EC were used interchangeably (Jeong et al. 2004). In terms of different analytical methodology, thermal EC and optical BC were determined by TOR analysis and optical attenuation methods (AE31) as mentioned before, respectively. To evaluate the agreement between thermal EC and optical BC concentrations in this study, an inter-comparison was conducted in Fig. S1. Twenty-four-hour average BC data were calculated to match the daily EC samples. Both strong correlations ($R = 0.80$ in XA and $R = 0.71$ in HK) and appropriate slopes ($S = 1.10$ in XA and $S = 0.95$ in HK) of the least-squares regression line passing through the origin of the plot, indicating that the concentrations were similar, and therefore, the two techniques produce results demonstrated a very good agreement of the TOR-EC and Optical-BC methods.

The $PM_{2.5}$ water-soluble potassium (K^+) concentrations were determined using a two-step protocol, including extraction of the WS-K^+ from the $PM_{2.5}$ water-soluble components and detection of the WS-K^+ concentration by an ion chromatograph (IC, Dionex 600, Dionex Corp, USA). Descriptions of the pretreatment of $PM_{2.5}$ filters for IC analysis and IC detection limitation are provided in our earlier studies (Shen et al. 2007; Zhang et al. 2015).

Potential source contribution function

The potential source contribution function (PSCF) can distinguish the different positions of the BC sources and their relative contributions. Based on the statistics of the backward air mass trajectories using the TrajStat software from the open-source GIS component MapWindow GIS ActiveX control (MapWindow open-source team, 2007) (Wang et al. 2009) and meteorological data from the NCEP Global Data Assimilation System (GDAS) (1° × 1°). The trajectory endpoints were 34.62° N and 108.93° E in XA and was 22.25° N and 114.25° E in HK, respectively, with a height of 500 m above ground level (i.e., the potential sources of different grid points can be estimated by Eq. 7 (Ashbaugh 1983)). The PSCF value for each grid point can be calculated as

$$\mathrm{PSCF} = M/N \tag{7}$$

where the PSCF was computed as a ratio of the selected grid points of high-BC events (M) to the total grid points of BC (N). The high-BC events were selected when the sample concentrations at the receptor site are higher than the criterion value (Wang et al. 2016). The PSCF results for the Aethalometer-generated BC source contributions (including BC_BB and BC_FF) were plotted in Fig. 4a–d. The criterion values for ambient BC_BB and BC_FF were chosen for the 75% percentile value for the entire period between XA and HK. Thus, the higher PSCF index in this study corresponds to the greater possible sources of BC_BB and BC_FF (Fleming et al. 2012; Karaca et al. 2009; Petroselli et al. 2018). The geographic area covered by the trajectories was divided into 814 grid cells of 0.5° latitude × 0.5° longitude in XA and 436 grid cells with the same resolution in HK.

The ME-2

Positive matrix factorization (PMF) is a widely used source apportionment model (Jaeckels et al. 2007; Kim et al. 2003; Xu et al. 2016a). This model solves a non-negativity constrained bilinear mass balance model using a weighted explicit least-squares equation (Paatero 1997). The principle of this model was listed in the following Eq. (8):

$$x_{ij} = \sum_{k=1}^{p} g_{i,k} f_{kj} + e_{ij} \tag{8}$$

where x_{ij} represents the jth species concentration measured in the ith sample, which can be decomposed into the $i*k$ matrix of g and $k*j$ matrix of f. The subscript i corresponds to the number of samples, j to the number of species, and p to the appropriate number of the sources. eij represents to $i*j$ matrix of residuals.

However, Paatero et al. (2002) found that the PMF model solution was not unique due to rotational ambiguity. Thus, the algorithm of ME-2 was developed to tackle PMF limitation when analyzing the structure of the energy sources and other environmental parameters. The key point of ME-2 was to minimize the objective function Q using a structural equation (Amato et al. 2009; Kuo et al. 2014; Paatero 1999):

$$Q = \sum_{i=1}^{m}\sum_{j=1}^{n}\left(\frac{e_{ij}}{\sigma_{ij}}\right)^2 \quad (9)$$

where σij is the measurement uncertainties of the jth species concentration in the ith sample, n is the number of samples, and m is the number of species. The calculation of σij was described in detail in Kuo et al. (2014) study.

Results and discussion

BC levels and relationship to $PM_{2.5}$ mass concentration

The time-resolved (1 h) variations of online $PM_{2.5}$ and BC at the two sampling sites and the BC/$PM_{2.5}$ ratio during sampling days were shown in Fig. 2. Large differences in $PM_{2.5}$ and BC mass concentration were observed between XA and HK. Moreover, the XA site had higher levels of BC and $PM_{2.5}$ mass loadings than the HK site. During sampling days (Table 1), XA daily $PM_{2.5}$ levels varied from 19 to 635 μg·m^{-3}, with an average of 182 ± 80.5 μg·m^{-3}. Additionally, XA BC concentration averaged 7.9 ± 3.3 μg·m^{-3}, and ranged from 0.8 to 25.3 μg·m^{-3}. The daily and diurnal trend between $PM_{2.5}$ and BC at XA was quite similar (Fig. 2). Specifically, it peaked during two heavily polluted periods of 18–21 Dec. 2016 and 30 Dec. 2016–6 Jan. 2017, when the meteorological conditions were stable. However, much lower values of $PM_{2.5}$ and BC were observed (34.5 ± 9.3 and 3.2 ± 0.9 μg·m^{-3}) in HK during the measurement periods. In comparison, the daily HK $PM_{2.5}$ and BC concentrations showed narrow concentration distributions, and both closely tracked the diurnal pattern of vehicle emissions, peaking during morning (7:00–10:00) and evening (16:00–18:00) rush hours, respectively (Fig. 2).

On average, the contribution of BC to $PM_{2.5}$ in HK was 10.7%, which was ~1.5 times that in XA (7.6%). Interestingly, lower XA BC/$PM_{2.5}$ ratios were observed on heavier polluted days, such as 2.9% on 21 Dec. 2016. In contrast, relatively higher XA BC/$PM_{2.5}$ ratios occurred during light-polluted periods, such as 22 Dec. (23%) and 27 Dec. (18%). These phenomena indicated that XA BC presented at fairly constant levels as a primary pollutant during sampling periods and was a major constituent of $PM_{2.5}$ during light-polluted periods. In HK, the relative high BC/$PM_{2.5}$ was observed during clear (on 27 Dec., 61.4% with low-$PM_{2.5}$ value) and polluted periods (on 21 Dec., 20.7% with high-$PM_{2.5}$ value), indicating that BC was an important component in HK $PM_{2.5}$.

The diurnal patterns of XA and HK BC were divided into three specific time periods: including daytime (6:00–18:00), nighttime (18:00–6:00), and peak traffic times (6:00–10:00

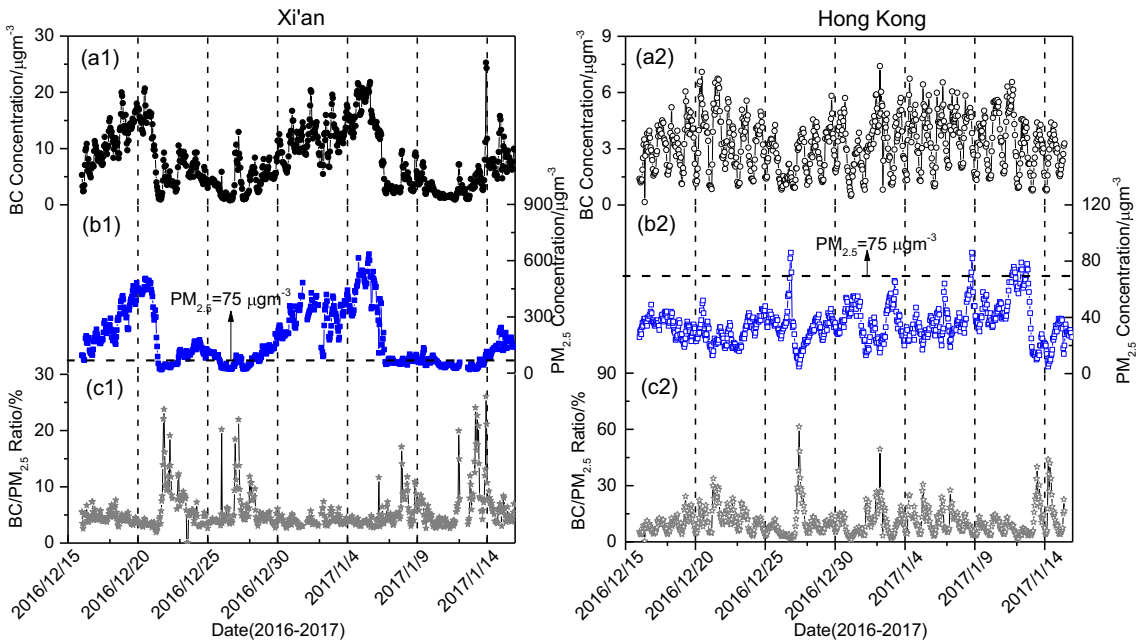

Fig. 2 Time-series plots of hourly averaged (a) BC concentrations, (b) $PM_{2.5}$ mass concentrations, and (c) BC/$PM_{2.5}$ ratios between Xi'an and Hong Kong. The horizontal black dashed line shows the grade 2 standard value for daily $PM_{2.5}$ concentration (75 μg m^{-3}) promulgated as the China National Ambient Air Quality Standard (GB 3095–2012)

Table 1 Concentrations for the major chemical species in $PM_{2.5}$ between Xi'an and Hong Kong

	Xi'an ($n = 30$)		Hong Kong ($n = 30$)	
	Mass, μg·m^{-3}		Mass, μg·m^{-3}	
	Average	SD	Average	SD
$PM_{2.5}$	182.0	80.5	34.5	9.3
BC	8.0	3.3	3.2	0.9
K^+	2.6	2.0	0.4	0.2
OC1	2.1	1.5	0.4	0.2
OC2	5.5	3.1	1.4	0.3
OC3	7.7	4.4	1.7	0.6
OC4	5.0	2.6	0.7	0.1
EC1	16.6	13.2	5.9	1.3
EC2	0.4	0.1	0.3	0.0
EC3	0.0	0.0	0.0	0.0
OP2	7.2	7.0	0.9	0.6

n sample numbers, *SD* standard deviation

and 17:00–21:00) (as shown in Fig. 3). In XA (Fig. 3a), similar values of BC can be found during different time periods with slightly higher values at night: nighttime (7.2 ± 3.0 μg·m^{-3}) > peak traffic (6.1 ± 2.8 μg·m^{-3}) and daytime (6.1 ± 2.9 μg·m^{-3}). These phenomena suggested that the XA BC was relatively stable across different time periods. However, the relative high nighttime BC values in XA emphasized the contribution of diesel trucks in construction sites, which were allowed work only in the evening (Xu et al. 2016b). As shown in Fig. 3b, HK BC during all sampling days was nearly threefold lower than in XA. Unlike the XA BC pattern, the HK BC displayed distinct levels during different sampling periods. For example, the mean values of HK BC in daytime and peak traffic times were 3.8 ± 1.1 and 3.7 ± 1.2 μg·m^{-3}, which were ~2.2 times higher than the nighttime HK BC value (1.6 ± 0.4 μg·m^{-3}). It indicated that traffic emissions had a significant effect on their ambient BC concentration. Specifically, much wider ranges were apparent during peak traffic times (2.5 μg·m^{-3} (minimum) and 4.4 μg·m^{-3} (maximum)), while the changes in BC distribution during non-traffic time at night were stable, mainly due to the lower traffic density.

Potential sources of BC between XA and HK

Using the results of data from procedures performed in the section "BC measurement and source identification," the sources of ambient BC in this study can be divide into two fractions, including fossil fuel combustion (i.e., vehicle exhaust and other industrial activities) and biomass burning (Cao et al. 2006a; Li et al. 2016; VanderWerf et al. 2006). Based on Eqs. 1–6 results, the high-BC_FF fractions (> 70%) were calculated in XA and HK, indicating that fossil fuel combustion was the dominant contributor to ambient BC at sampling site. The relatively high BC_BB of 25.8% was observed in XA during our sampling periods. Conversely, the lowest HK BC_BB fraction (16.4%) was obtained in HK with minimal biomass burning contributions.

In XA, high-criterion values of BC_FF (refer to the 75% of all XA BC_FF data, > 3.6 μg·m^{-3}) and BC_BB (> 1.2 μg·m^{-3}) were used to improve the resolution of PSCF source identifications. As shown in Fig. 4a, b, the XA PSCF results with 500-m height were slightly different between BC_FF and BC_BB. The XA sampling site was surrounded by the region with high-PSCF (0.8–1) values, emphasizing that the local

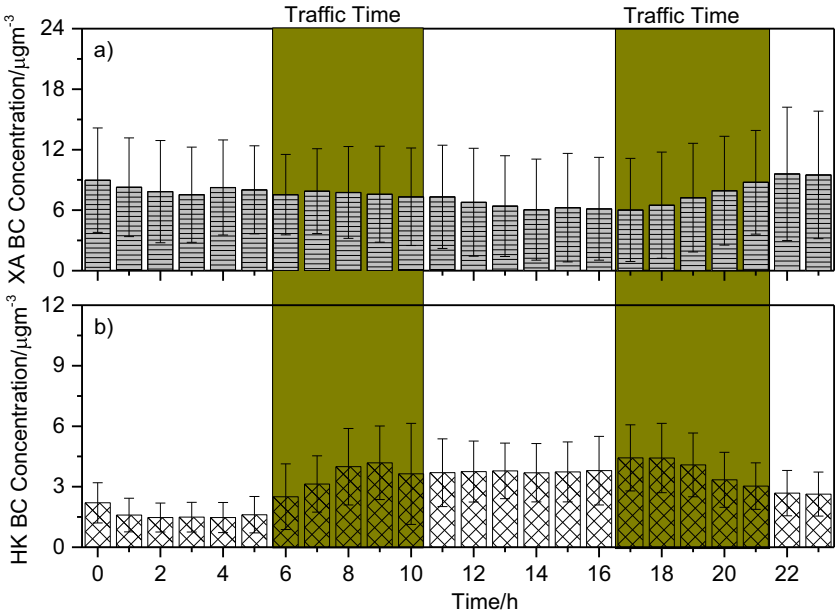

Fig. 3 The diurnal variations of BC between **a** Xi'an and **b** Hong Kong (The red dots represent the diurnal BC range and the error bars represent one standard deviation of BC concentration)

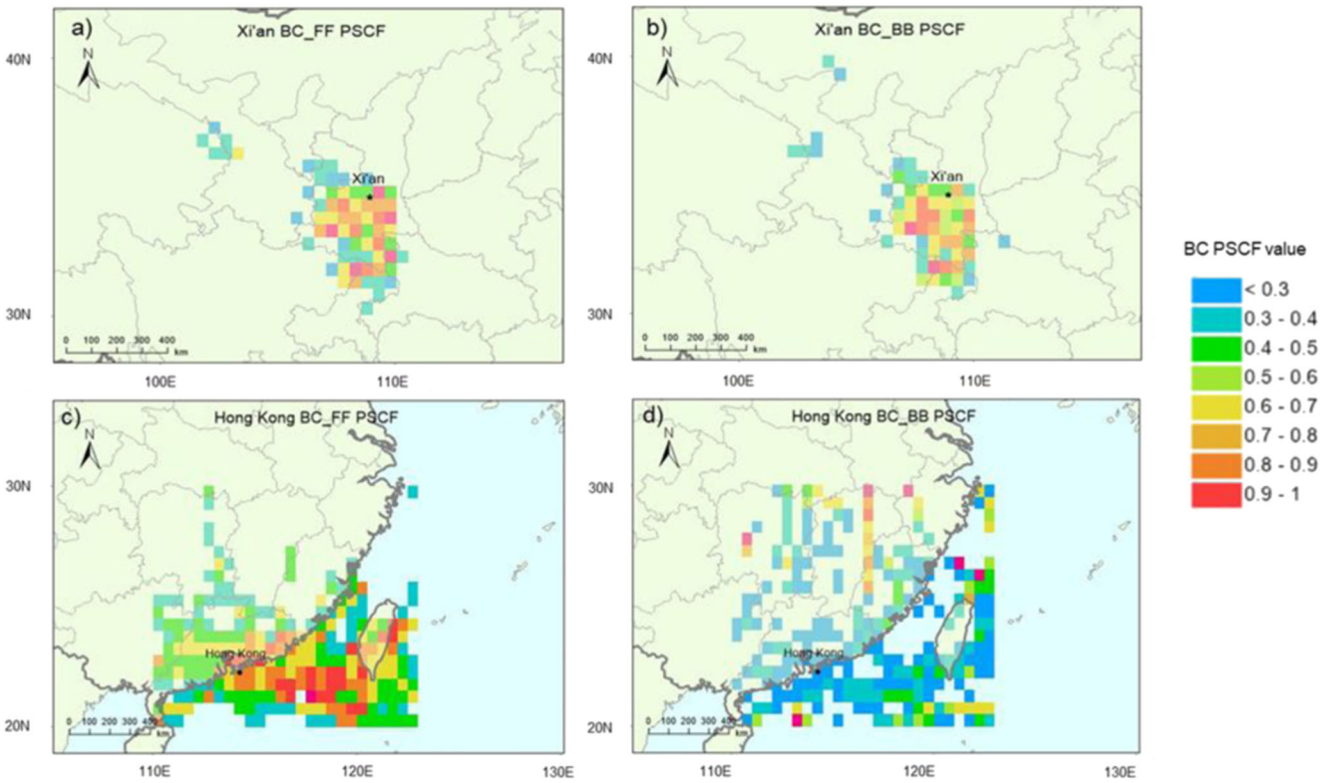

Fig. 4 Seventy-fifth percentile PSCF probabilities of Aethalometer-generated BC fractions computed using respectively **a** Xi'an BC_FF, **b** Xi'an BC_BB, **c** Hong Kong BC_FF, and **d** Hong Kong BC_BB trajectories reaching the sites during sampling periods. The trajLevel smoothing was disabled to better identify the originating trajectories

emissions play an important role in both BC_FF and BC_BB loadings. In addition, the highest BC_BB PSCF values of 0.7–0.9 were observed in the southwest XA. These areas include the suburbs, where there is a high-amount biomass burning (Sun et al. 2017).

As shown in Fig. 4c, d, the range of important potential source region for BC observed in HK was wider than those in XA at the height of 500 m. The values of 1.4 $\mu g \cdot m^{-3}$ and 0.5 $\mu g \cdot m^{-3}$ were calculated as criterion values for HK BC_FF and BC_BB PSCF analysis, respectively. High-HK BC_FF PSCF range (0.6–1.0) was addressed, of which area was regarded as short-range flow from the northeast of HK. This area includes the coastal cities of Xiamen, Shantou, and Shanwei, which are known to have high and numerous industrial fossil fuel BC sources (Wang et al. 2016; Zhang et al. 2009). It should also be noted that in addition to the influences from these cities, there are possible maritime contributions to BC_FF by heavy commercial shipping traffic in coastal waters (Lack and Corbett 2012). The highest HK BC_FF PSCF regions observed in the eastern direction of HK. These heavily polluted BC_FF mass clusters generally originated from Taiwan at a high altitude, then mixed down when traveling above the sea. Further, both west and NW directions were the important potential source regions for HK BC_FF, verifying that heating emissions (i.e., coal combustion) from northern China also contribute to HK BC_FF. As concluded in Fig. 4d, the concentration of biomass burning to BC was limited due to low-PSCF BC_BB values (0.2–0.3). A few areas with high-PSCF ranges of BC_BB (greater than 0.7) were observed in the northern directions of HK possibly because the rural areas in Jiangxi and Fujian province emissions of anthropogenic contaminants (wood combustion/biomass burning) and those pollutants could be carried by north-prevailing winds to HK BC_BB.

BC source apportionment

As mentioned above, the primary sources contributed significantly to the BC concentration between XA and HK regions. To assess the contributions from these sources, the typical source markers are believed to be of low volatility and reasonably stable in the atmosphere under wintertime conditions for use as fitting species. The concentration and relative standard deviation data of water-soluble non-organic ion (K^+), eight thermal carbonaceous fractions (i.e., OC1, OC2, OC3, OC4, EC1, EC2, EC3, and OP), and BC were listed in Table 1 and input into the ME-2 software. After analysis, three anthropogenic sources of BC over sampling sites were selected: (1) coal emissions, (2) motor vehicle emissions, and (3) biomass burning.

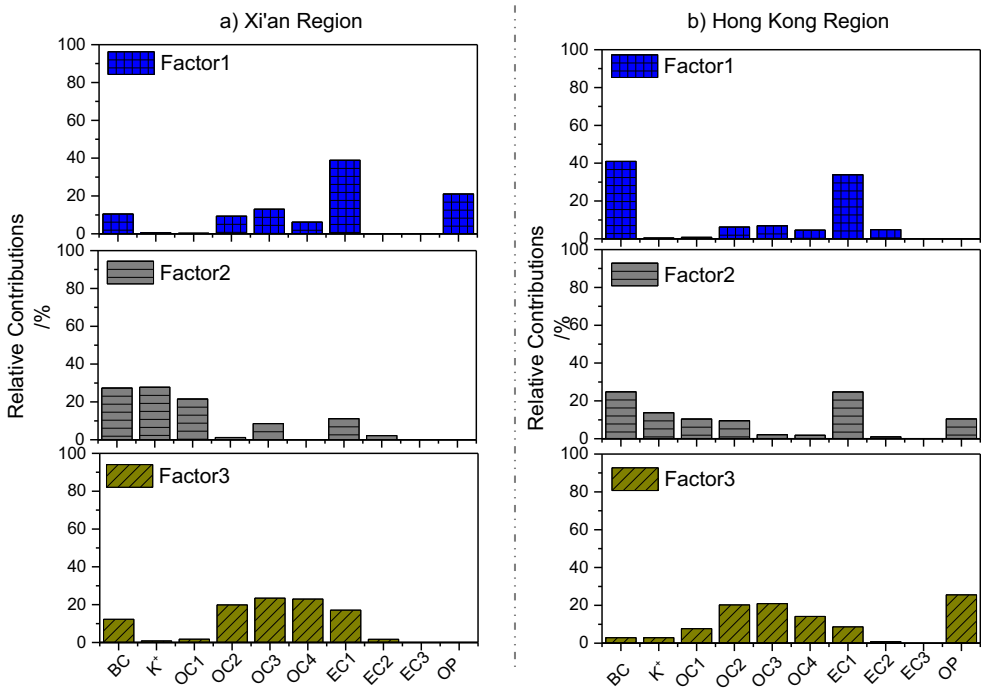

Fig. 5 Comparisons of fractional contributions of the factors retrieved by ME-2 to the primary $PM_{2.5}$'s markers between **a** Xi'an and **b** Hong Kong

In Fig. 5a, the factors of XA BC can be identified as follows: (1) factor 1 had high loadings of OC2 (9.3%), OC3 (13.0%), OC4 (6.2%), and EC1 (38.9%), and it was identified as vehicle source because these species are typically emitted by motor vehicles (Cao et al. 2005; Chow et al. 2004). (2) Factor 2 representing open or smoldering burns of various types of wood or maize straw burning contained an abundance of water-soluble K^+, marker for vegetative burning (Cheng et al. 2013; Cheng et al. 2014; Shen et al. 2007), at the level of 27.8%. Sun et al. (2017) have pointed out that smoldering straw burning in winter in suburban areas of XA produces more OC1, and this could explain a larger OC1 fraction (21.6%) in factor 2. (3) Factor 3 in this study was highly loaded with OC2, OC3, and OC4, and it was identified as coal burning because these species are typically enriched in coal-fired boiler and residential stoves burning coal samples (Cao et al. 2005; Chow et al. 2004). The results of Primary-HK $PM_{2.5}$ were also summarized in Fig. 5b. The proportions of EC1 + OC2 + OC3 and OC4 + EC2 were high in factor 1 in HK, which appear to represent gasoline and diesel exhaust, respectively (Cao et al. 2006b). Similar to XA factor 2, high loadings of water-soluble K^+ and OC1 indicated the biomass burning (Chow et al. 2005). Also, pyrolyzed OC (OP) was reported to be a slightly high in factor 2, which has to be proven to be associated with water-soluble OC (Ni et al. 2015; Yang and Yu 2002) and was mainly emitted from smoldering, straw-residue fires (Sun et al. 2017; Sun et al. 2018). In HK $PM_{2.5}$, factor 3 was highly loaded with OC2, OC3, and OC4, which appears to represent coal burning.

Based on ME-2 analysis, the source contributions to XA BC were assessed in Fig. 6a. In XA, vehicle emissions were the largest source of BC, accounting for 32.9% of the BC mass. This may have been induced by the rapidly increased vehicle traffic and energy consumption during the past several decades in XA. Moreover, coal combustion during winter was the second largest contributor of BC, accounting for 22.5%. Further, 19.6% of XA BC originated from biomass burning.

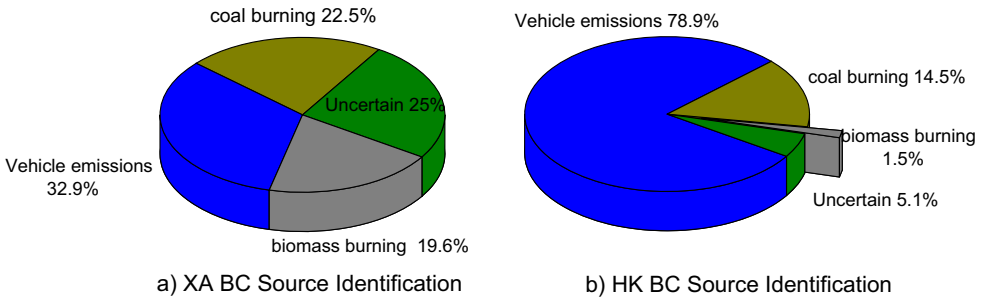

Fig. 6 Source contributions to **a** XA and **b** HK BC

The majority of biomass burning in this area consisted of traditional maize straw burning during winter to heat rural residences. Indeed, maize straw moldering in "Heated Kang" leads to a great deal of rural and urban air pollution (Sun et al. 2017). As shown in Fig. 6b, vehicle emissions accounted for the largest fraction of BC (78.9%) in HK. However, low but non-neglected fractions of biomass (1.5%) and coal burning (14.5%) were observed in HK BC, which can be attributed to transport the mainland that would bring these emissions to HK. These conclusions were also supported by the HK BC transport pathways from northern China.

Conclusion

The results showed that the mean concentration of BC was 7.9 $\mu g \cdot m^{-3}$ in XA and was 3.2 $\mu g \cdot m^{-3}$ in HK during the sampling periods. In XA, the highest BC concentration was 25.3 $\mu g \cdot m^{-3}$, while the lowest value was 0.8 $\mu g \cdot m^{-3}$, indicating that XA BC varied greatly on a daily scale. In contrast, the daily HK BC concentration distribution showed much lower variations. For the temporal variations of BC, stable and high-BC levels were obtained in XA compared to those in HK. However, the distribution of HK BC was more sensitive to traffic flow. PSCF analysis showed that XA BC was mainly influenced by local anthropogenic sources while HK BC was heavily influenced by transport of emissions from remote coastal cities and ocean ships. We quantified the BC sources according to the relationships among BC, $PM_{2.5}$ chemical compositions, and various sources and found that the main sources of XA BC were biomass burning, coal burning, and mobile exhaust emissions, while the HK BC was mainly originated from vehicle emissions.

Funding information This research was supported by the National Natural Science Foundation of China (41573101), and a grant from SKLLQG, Chinese Academy of Sciences (SKLLQG1616). This research was also supported by the grant from the Research Grants Council of the Hong Kong Special Administrative Region, China (RGC Project No. 21201214).

References

Allen GA, Lawrence J, Koutrakis P (1999) Field validation of a semi-continuous method for aerosol black carbon (aethalometer) and temporal patterns of summertime hourly black carbon measurements in southwestern PA. Atmos Environ 33:817–823

Amato F, Pandolfi M, Escrig A, Querol X, Alastuey A, Pey J, Perez N, Hopke P (2009) Quantifying road dust resuspension in urban environment by multilinear engine: a comparison with PMF2. Atmos Environ 43:2770–2780

Ashbaugh LL (1983) A statistical trajectory technique for determining air pollution source regions. J Air Pollut Control Associ 33:1096–1098

Bond TC, Doherty SJ, Fahey D, Forster P, Berntsen T, DeAngelo B, Flanner M, Ghan S, Kärcher B, Koch D (2013) Bounding the role of black carbon in the climate system: a scientific assessment. J Geophys Res 118:5380–5552

Cao J, Lee S, Ho K, Zou S, Zhang X, Pan J (2003) Spatial and seasonal distributions of atmospheric carbonaceous aerosols in pearl river delta region, China. China Particuol 1:33–37

Cao JJ, Wu F, Chow JC, Lee SC, Li Y, Chen SW, An ZS, Fung KK, Watson JG, Zhu CS, Liu SX (2005) Characterization and source apportionment of atmospheric organic and elemental carbon during fall and winter of 2003 in Xi'an, China. Atmos Chem Phys 5(11): 3127–3137

Cao G, Zhang X, Zheng F (2006a) Inventory of black carbon and organic carbon emissions from China. Atmos Environ 40:6516–6527

Cao J, Lee S, Ho K, Fung K, Chow JC, Watson JG (2006b) Characterization of roadside fine particulate carbon and its eight fractions in Hong Kong. Aerosol Air Qual Res 6:106–122

Cheng Y, Lee S, Ho K, Chow J, Watson J, Louie P, Cao J, Hai X (2010) Chemically-speciated on-road $PM_{2.5}$ motor vehicle emission factors in Hong Kong. Sci Total Environ 408:1621–1627

Cheng Y, Engling G, He KB, Duan FK, Ma YL, Du ZY, Liu JM, Zheng M, Weber RJ (2013) Biomass burning contribution to Beijing aerosol. Atmos Chem Phys 13:7765–7781

Cheng Z, Wang S, Fu X, Watson J, Jiang J, Fu Q, Chen C, Xu B, Yu J, Chow J (2014) Impact of biomass burning on haze pollution in the Yangtze River delta, China: a case study in summer 2011. Atmos Chem Phys 14:4573–4585

Chow JC, Watson JG, Kuhns H, Etyemezian V, Lowenthal DH, Crow D, Kohl SD, Engelbrecht JP, Green MC (2004) Source profiles for industrial, mobile, and area sources in the Big Bend Regional Aerosol Visibility and Observational study. Chemosphere 54:185–208

Chow JC, Watson JG, Louie PK, Chen LW, Sin D (2005) Comparison of $PM_{2.5}$ carbon measurement methods in Hong Kong, China. Environ Pollut 137:334–344

Collaud CM, Weingartner E, Apituley A, Ceburnis D, Fierz-Schmidhauser R, Flentje H, Henzing J, Jennings SG, Moerman M, Petzold A (2010) Minimizing light absorption measurement artifacts of the Aethalometer: evaluation of five correction algorithms. Atmos Meas Tech 3:457–474

Cooke WF, Wilson JJ (1996) A global black carbon aerosol model. J Geophys Res Atmos 101:19395–19409

Ding A, Huang X, Nie W, Sun J, Kerminen VM, Petäjä T, Su H, Cheng Y, Yang XQ, Wang M (2016) Enhanced haze pollution by black carbon in megacities in China. Geophys Res Lett 43:2873–2879

Fleming ZL, Monks PS, Manning AJ (2012) Untangling the influence of air-mass history in interpreting observed atmospheric composition. Atmos Res 104:1–39

Healy R, Sofowote U, Su Y, Debosz J, Noble M, Jeong CH, Wang J, Hilker N, Evans G, Doerksen G (2017) Ambient measurements and source apportionment of fossil fuel and biomass burning black carbon in Ontario. Atmos Environ 161:34–47

Huang K, Zhuang G, Lin Y, Wang Q, Fu JS, Zhang R, Li J, Deng C, Fu Q (2012) Impact of anthropogenic emission on air quality over a megacity–revealed from an intensive atmospheric campaign during the Chinese Spring Festival. Atmos Chem Phys 12:11631–11645

Jaeckels JM, Bae MS, Schauer JJ (2007) Positive matrix factorization (PMF) analysis of molecular marker measurements to quantify the sources of organic aerosols. Environ Sci Technol 41:5763–5769

Jeong CH, Hopke PK, Kim E, Lee DW (2004) The comparison between thermal-optical transmittance elemental carbon and Aethalometer black carbon measured at multiple monitoring sites. Atmos Environ 38:5193–5204

Karaca F, Anil I, Alagha O (2009) Long-range potential source contributions of episodic aerosol events to PM_{10} profile of a megacity. Atmos Environ 43:5713–5722

Kim E, Larson TV, Hopke PK, Slaughter C, Sheppard LE, Claiborn C (2003) Source identification of $PM_{2.5}$ in an arid northwest US city by positive matrix factorization. Atmos Res 6:291–305

Kirchstetter TW, Aguiar J, Tonse S, Fairley D, Novakov T (2008) Black carbon concentrations and diesel vehicle emission factors derived from coefficient of haze measurements in California: 1967–2003. Atmos Environ 42:480–491

Kuo CP, Liao HT, Chou CCK, Wu CF (2014) Source apportionment of particulate matter and selected volatile organic compounds with multiple time resolution data. Sci Total Environ 472:880–887

Lack D, Corbett J (2012) Black carbon from ships: a review of the effects of ship speed, fuel quality and exhaust gas scrubbing. Atmos Chem Phys 12:3985–4000

Lee YL, Sequeira R (2002) Water-soluble aerosol and visibility degradation in Hong Kong during autumn and early winter, 1998. Environ Pollut 116:225–233

Li B, Gasser T, Ciais P, Piao S, Tao S, Balkanski Y, Hauglustaine D, Boisier JP, Chen Z, Huang M, Li LZ, Li Y, Liu H, Liu J, Peng S, Shen Z, Sun Z, Wang R, Wang T, Yin G, Yin Y, Zeng H, Zeng Z, Zhou F (2016) The contribution of China's emissions to global climate forcing. Nature 531:357–361

Lin Y, Huang K, Zhuang G, Fu JS, Wang Q, Liu T, Deng C, Fu Q (2014) A multi-year evolution of aerosol chemistry impacting visibility and haze formation over an Eastern Asia megacity, Shanghai. Atmos Environ 92:76–86

Lloyd AC, Cackette TA (2001) Diesel engines: environmental impact and control. J Air Waste Manag Assoc 51:809–847

Ni H, Han Y, Cao J, Chen LWA, Tian J, Wang X, Chow JC, Watson JG, Wang Q, Wang P (2015) Emission characteristics of carbonaceous particles and trace gases from open burning of crop residues in China. Atmos Environ 123:399–406

Ning Z, Chan K, Wong K, Westerdahl D, Močnik G, Zhou J, Cheung C (2013) Black carbon mass size distributions of diesel exhaust and urban aerosols measured using differential mobility analyzer in tandem with Aethalometer. Atmos Environ 80:31–40

Paatero P (1997) Least squares formulation of robust non-negative factor analysis. Chemometrics Intell Lab 37:23–35

Paatero P (1999) The multilinear engine-a table-driven, least squares program for solving multilinear problems, including the n-way parallel factor analysis model. J Comput Graph Stat 8:854–888

Paatero P, Hopke PK, Song XH, Ramadan Z (2002) Understanding and controlling rotations in factor analytic models. Chemometrics Intell Lab 60:253–264

Pérez N, Pey J, Cusack M, Reche C, Querol X, Alastuey A, Viana M (2010) Variability of particle number, black carbon, and PM_{10}, $PM_{2.5}$, and PM_1 levels and speciation: influence of road traffic emissions on urban air quality. Aerosol Sci Technol 44:487–499

Petroselli C, Crocchianti S, Moroni B, Castellini S, Selvaggi R, Nava S, Galzolai G, Lucarelli F, Cappelletti D (2018) Disentangling the major source areas for an intense aerosol advection in the Central Mediterranean on the basis of Potential Source Contribution Function modeling of chemical and size distribution measurements. Atmos Res 204:67–77

Ramanathan V, Carmichael G (2008) Global and regional climate changes due to black carbon. Nat Geosci 1:221–227

Reddy CM, Pearson A, Xu L, McNichol AP, Benner BA, Wise SA, Klouda GA, Currie LA, Eglinton TI (2002) Radiocarbon as a tool to apportion the sources of polycyclic aromatic hydrocarbons and black carbon in environmental samples. Environ Sci Technol 36: 1774–1782

Sandradewi J, Prévôt AS, Szidat S, Perron N, Alfarra MR, Lanz VA, Weingartner E, Baltensperger U (2008) Using aerosol light absorption measurements for the quantitative determination of wood burning and traffic emission contributions to particulate matter. Environ Sci Technol 42:3316–3323

Shen ZX, Cao JJ, Arimoto R, Zhang RJ, Jie DM, Liu SX, Zhu CS (2007) Chemical composition and source characterization of spring aerosol over Horqin sand land in northeastern China. J Geophys Res 112:D14315

Shen Z, Zhang L, Cao J, Tian J, Liu L, Wang G, Zhao Z, Wang X, Zhang R, Liu S (2012) Chemical composition, sources, and deposition fluxes of water-soluble inorganic ions obtained from precipitation chemistry measurements collected at an urban site in northwest China. J Environ Monit 14:3000–3008

Shen Z, Zhang Q, Cao J, Zhang L, Lei Y, Huang Y, Huang RJ, Gao J, Zhao Z, Zhu C (2016) Optical properties and possible sources of brown carbon in $PM_{2.5}$ over Xi'an, China. Atmos Environ 150:322–330

Shen Z, Lei Y, Zhang L, Zhang Q, Zeng Y, Tao J, Zhu C, Cao J, Xu H, Liu S (2017) Methanol extracted brown carbon in $PM_{2.5}$ over Xi'an, China: seasonal variation of optical properties and sources identification. Aerosol Sci Eng 1(2):57–65

Shindell D, Kuylenstierna JCI, Vignati E, van Dingenen R, Amann M, Klimont Z, Anenberg SC, Muller N, Janssens-Maenhout G, Raes F, Schwartz J, Faluvegi G, Pozzoli L, Kupiainen K, Höglund-Isaksson L, Emberson L, Streets D, Ramanathan V, Hicks K, Oanh NTK, Milly G, Williams M, Demkine V, Fowler D (2012) Simultaneously mitigating near-term climate change and improving human health and food security. Science 335:183–189

Sun J, Shen Z, Cao J, Zhang L, Wu T, Zhang Q, Yin X, Lei Y, Huang Y, Huang R (2017) Particulate matters emitted from maize straw burning for winter heating in rural areas in Guanzhong Plain, China: current emission and future reduction. Atmos Res 184:66–76

Sun J, Shen Z, Zhang L, Zhang Q, Lei Y, Cao J, Huang Y, Liu S, Zheng C, Xu H (2018) Impact of primary and secondary air supply intensity in stove on emissions of size-segregated particulate matter and carbonaceous aerosols from apple tree wood burning. Atmos Res 202:33–39

VanderWerf GR, Randerson JT, Giglio L, Collatz GJ, Kasibhatla PS, Arellano AF Jr (2006) Interannual variability in global biomass burning emissions from 1997 to 2004. Atmos Chem Phys 6:3423–3441

Virkkula A, Mäkelä T, Hillamo R, Yli-Tuomi T, Hirsikko A, Hämeri K, Koponen IK (2007) A simple procedure for correcting loading effects of aethalometer data. J Air Waste Manage Assoc 57:1214–1222

Wang Y, Zhang X, Draxler RR (2009) TrajStat: GIS-based software that uses various trajectory statistical analysis methods to identify potential sources from long-term air pollution measurement data. Environ Model Softw 24:938–939

Wang R, Tao S, Shen H, Wang X, Li B, Shen G, Wang B, Li W, Liu X, Huang Y (2012a) Global emission of black carbon from motor vehicles from 1960 to 2006. Environ Sci Technol 46:1278–1284

Wang R, Tao S, Wang W, Liu J, Shen H, Shen G, Wang B, Liu X, Li W, Huang Y (2012b) Black carbon emissions in China from 1949 to 2050. Environ Sci Technol 46:7595–7603

Wang R, Tao S, Shen H, Huang Y, Chen H, Balkanski Y, Boucher O, Ciais P, Shen G, Li W (2014) Trend in global black carbon emissions from 1960 to 2007. Environ Sci Technol 48:6780–6787

Wang Q, Liu S, Zhou Y, Cao J, Han Y, Ni H, Zhang N, Huang R (2015) Characteristics of black carbon aerosol during the Chinese Lunar Year and weekdays in Xi'an, China. Atmosphere 6:195–208

Wang Q, Huang RJ, Zhao Z, Zhang N, Wang Y, Ni H, Tie X, Han Y, Zhuang M, Wang M, Zhang J, Zhang X, Dusek U, Cao J (2016) Size distribution and mixing state of refractory black carbon aerosol from a coastal city in South China. Atmos Res 181:163–171

World Health Organization (WHO) (2012) Health effects of black carbon. WHO, Geneva

Xu H, Cao J, Chow JC, Huang RJ, Shen Z, Chen LA, Ho KF, Watson JG (2016a) Inter-annual variability of wintertime $PM_{2.5}$ chemical composition in Xi'an, China: evidences of changing source emissions. Sci Total Environ 545:546–555

Xu H, Ho SSH, Gao M, Cao J, Guinot B, Ho KF, Long X, Wang J, Shen Z, Liu S (2016b) Microscale spatial distribution and health assessment of $PM_{2.5}$-bound polycyclic aromatic hydrocarbons (PAHs) at nine communities in Xi'an, China. Environ Pollut 218:1065–1073

Yang H, Yu JZ (2002) Uncertainties in charring correction in the analysis of elemental and organic carbon in atmospheric particles by thermal/optical methods. Environ Sci Technol 36:5199–5204

Zhang Q, Streets DG, Carmichael GR, He K, Huo H, Kannari A, Klimont Z, Park I, Reddy S, Fu J (2009) Asian emissions in 2006 for the NASA INTEX-B mission. Atmos Chem Phys 9:5131–5153

Zhang Q, Shen Z, Cao J, Zhang R, Zhang L, Huang RJ, Zheng C, Wang L, Liu S, Xu H (2015) Variations in $PM_{2.5}$, TSP, BC, and trace gases (NO_2, SO_2, and O_3) between haze and non-haze episodes in winter over Xi'an, China. Atmos Environ 112:64–71

Zhang Q, Ning Z, Shen Z, Li G, Zhang J, Lei Y, Xu H, Sun J, Zhang L, Westerdahl D, Gali NK (2017) Variations of aerosol size distribution, chemical composition and optical properties from roadside to ambient environment: a case study in Hong Kong, China. Atmos Environ 166:34–243

Zotter P, Herich H, Gysel M, El-Haddad I, Zhang Y, Močnik G, Hüglin C, Baltensperger U, Szidat S, Prévôt AS (2017) Evaluation of the absorption Ångström exponents for traffic and wood burning in the Aethalometer-based source apportionment using radiocarbon measurements of ambient aerosol. Atmos Chem Phys 17:4229–4249